Vol 17 No 10, October 2008
1674-1056/2008/17(10)/3910-07

Chinese Physics B

© 2008 Chin. Phys. Soc.
and IOP Publishing Ltd

Multiferroic behaviour of epitaxial $NiFe_2O_4$–$BaTiO_3$ heterostructures*

Zhang Yi(张 毅), Deng Chao-Yong(邓朝勇), Ma Jing(马 静), Lin Yuan-Hua(林元华), and Nan Ce-Wen(南策文)†

Department of Materials Science and Engineering, State Key Laboratory of New Ceramics and Fine Processing, Tsinghua University, Beijing 100084, *China*

(Received 17 September 2007; revised manuscript received 24 October 2008)

Multiferroic $NiFe_2O_4$ (NFO)–$BaTiO_3$ (BTO) bilayered thin films are epitaxially grown on (001) Nb-doped $SrTiO_3$ (STO) substrates by pulsed-laser deposition (PLD). Different growth sequences of NFO and BTO on the substrate yield two kinds of epitaxial heterostructures with (001)-orientation, i.e. (001)-NFO/(001)-BTO/substrate and (001)-BTO/(001)-NFO/substrate. Microstructure studies from x-ray diffraction (XRD) and electron microscopies show differences between these two heterostructures, which result in different multiferroic behaviours. The heterostructured composite films exhibit good coexistence of both ferroelectric and ferromagnetic properties, in particular, obvious magnetoelectric (ME) effect on coupling response.

Keywords: magnetoelectric effect, epitaxial heterostructure, nickel ferrite, multiferroics
PACC: 7580, 8115I, 6865

1. Introduction

Multiferroic magnetoelectric (ME) materials can display not only ferroelectric and magnetic properties simultaneously, but also a coupling effect between the electric and magnetic polarizations,[1−3] that is, a spontaneous dielectric polarization induced by an external magnetic field (i.e. direct ME effect), or a magnetization induced by an applied electric field (i.e. converse ME effect). The basic requirement for observation of such a coupling ME effect is the coexistence of ferroelectric and ferromagnetic subsystems. With the exception of single phase multiferroic ME materials whose ME response is either too weak or occurs at too low a temperature for practical exploitation, composite systems such as combinations of piezoelectric ceramics [e.g. $BaTiO_3$ and lead-zirconate-titanate (PZT)] and ferrites or rare-earth-iron alloys (e.g., Terfenol-D) have been employed to obtain a large ME effect above room temperature.[4−7] These bulk ME composites are not amenable to on-chip integration, which is a prerequisite for their incorporation into microelectronic devices. Most recently, ME nanocomposite thin films[8] of ferroelectric and magnetic oxides have become a new route to such multiferroic composites. Compared with bulk composite thin films, ME composite supply more degrees of freedom, such as lattice strain or interlayer interaction, to change and optimize the ME behaviour. It also paves the way for investigating the physical mechanism of ME effect in nanoscale.

Different ME heterostructured films have been grown, i.e. vertical heterostructure (so-called 1-3 type structure) consisting of magnetic spinel pillars (e.g. $CoFe_2O_4$) vertically embedded into a ferroelectric perovskite matrix (e.g., $BaTiO_3$, $PbTiO_3$, or $BiFeO_3$), and horizontal nanostructures (2-2 type structure) consisting of alternating layers of a ferroelectric perovskite and magnetic oxides. The obvious ME coupling has been observed via microscopy in such vertical nanostructures,[9] through the switching of the magnetization on reversal of the ferroelectric polarization. But the direct ME measurement of such a vertical heterostructure (so-called 1-3 type structure) is difficult because of low resistance of $CoFe_2O_4$ pillars penetrating through the film. The theoretical researches[10−12] indicate that horizontally nanostructured (so-called 2-2 type structure) multiferroic films exhibit a much weaker ME effect than vertically heterostructured films due to a large in-plane constraint

*Project supported by the State Key Development Program for Basic Research of China (Grant No 2002CB613303) and the National High Technology Research and Development Program for Advanced Materials of China (Grant No 2006AA03Z101) and the National Natural Science Foundation of China (Grant Nos 10574078 and 50621201).
†Corresponding author. E-mail: cwnan@tsinghua.edu.cn

from substrates, but their ME effect could be comparable to that in their 2-2 type bulk counterparts.[13] Furthermore, the 2-2 type films are very easy to fabricate and rule out the leakage problem due to the ferroelectric layers, which leads to a visible direct ME effect. Although a large converse ME effect has been observed recently in the horizontal heterostructure of a ferromagnetic $LaSrMnO_3$ film grown on a single crystal $BaTiO_3$ substrate,[14] there have been made few convincing observations of the direct ME effect in a horizontal heterostructure.[13,15,16]

On the other hand, due to the difference in structure between magnetic phase (e.g. spinel $CoFe_2O_4$ or $NiFe_2O_4$) and ferroelectric phase (e.g., perovskite $BaTiO_3$), they have different growth mechanisms on oriented $SrTiO_3$(STO) substrates.[17] Thus, the growth sequences of the magnetic and the ferroelectric phases in the horizontal heterostructures should bring an influence on the structure and further on the multiferroic properties of thin films. In this paper, we report on the multiferroic behaviours in horizontally heterostructured films of $BaTiO_3$ (BTO) and $NiFe_2O_4$ (NFO), which are deposited in different growth sequences by using the pulse laser deposition (PLD) technique. NFO is chosen as the magnetic phase due to its smaller coercive field and larger resistivity, which could conduce to the rotation of magnetic domains and a reduction in leakage current. The results show that the growth sequences of BTO and NFO have an obvious effect on the multiferroic behaviours of the simple horizontally heterostructured films.

2. Experiment

A pulsed KrF excimer laser with a wavelength of 248 nm and an average energy density of about 1.5 J/cm^2 per pulse was employed for the deposition of the heterostructured thin films on (001) oriented 0.7% Nb-doped $SrTiO_3$ (STO). Two different heterostructure films were deposited, i.e. (1) the NFO/BTO films with BTO as the bottom layer on the substrate, and in a reverse order, (2) the BTO/NFO films with the bottom layer being NFO. The BTO was deposited from a BTO ceramic target at an O_2 pressure of 13 Pa and a substrate temperature of 1070 K. The NFO was deposited from an NFO ceramic target at the same O_2 pressure but a substrate temperature of 920 K. The pulse repetition rate was 5 Hz. The deposition rates for NFO and BTO were about 3 nm/min and 8 nm/min, respectively.

The film phases were characterized by using x-ray diffraction (XRD) (Rigaku D/max-2500 and Rigaku D/max-3A) with CuKa. Scanning electron microscope (SEM) (Hitachi S5500) and high resolution transmission electron microscope (HRTEM) (FEI Tecnai F30) were utilized for the observation of the film microstructures. For electric measurement, Pt electrode dots with 300 μm in diameter were deposited on the top surface. Electric measurement was carried out by using a TF analyzer2000 (aixACCT Co.). Magnetic properties were measured by using a superconducting quantum interference device (SQUID, MPMS-7) magnetometer. For magnetoelectric measurement, the film samples were electrically connected with silver wires bonded to the top Pt electrode and to the substrate separately. A dc bias magnetic field $H_{\rm dc}$ was superimposed by a small ac magnetic field δH in parallel. The values of induced voltage signal δV in the films were collected by a lock-in amplifier (EG&G 5210). All measurements were performed at room temperature.

3. Results and discussion

Two heterostructures, i.e. BTO/NFO/STO with NFO as the bottom layer on the (001)-oriented STO substrate, and in a reverse order, NFO/BTO/STO with BTO as the bottom layer, were grown. The thicknesses of the NFO layers in both heterostructures are about 40 nm. The thicknesses of the BTO layers in the BTO/NFO/STO and NFO/BTO/STO heterostructures are about 110 nm and 75 nm, respectively. As shown in Fig.1, there is no additional phase apart from NFO and BTO in these films. As marked in this figure, only the (00l) diffraction peaks appear in the XRD patterns of these films, indicating that the films are c-axis orientated. To further investigate the degree of in-plane orientations, the φ-scanned XRD was performed. As presented in Figs.1(b) and 1(c), the peaks for the NFO (404), BTO (202), and STO (202) reflections all appear at the same azimuthal angle φ, and the four peaks are 90 degree apart from each other. The interface relationship is determined as (001)-BTO // (001)-NFO // (001)-STO and [100]-BTO // [100]-NFO // [100]-STO, or (001)-NFO // (001)-BTO // (001)-STO and [100]-NFO // [100]-BTO // [100]-STO, from the in-plane orientations. There are some tiny peaks of NFO in

the ϕ scanned patterns for both NFO/BTO/STO and BTO/NFO/STO heterostructures, showing that the deposition of NFO (spinel structure) on STO or the BTO layer is not of an ideal "cube-on-cube" epitaxial growth, which might be attributed to the large lattice mismatch between the NFO and the STO substrate in the BTO/NFO/STO heterostructure. In order to reduce the large strain energy, some misfit edge dislocations form at the interface (see Fig.3(a) below), leading to a small change in the lattice direction of epitaxial growth. In the NFO/BTO/STO case, a bit rougher surface of the BTO bottom layer than that of the STO substrate may also be responsible for the small peaks of NFO in φ scanned pattern in addition to the contribution of the dislocations.

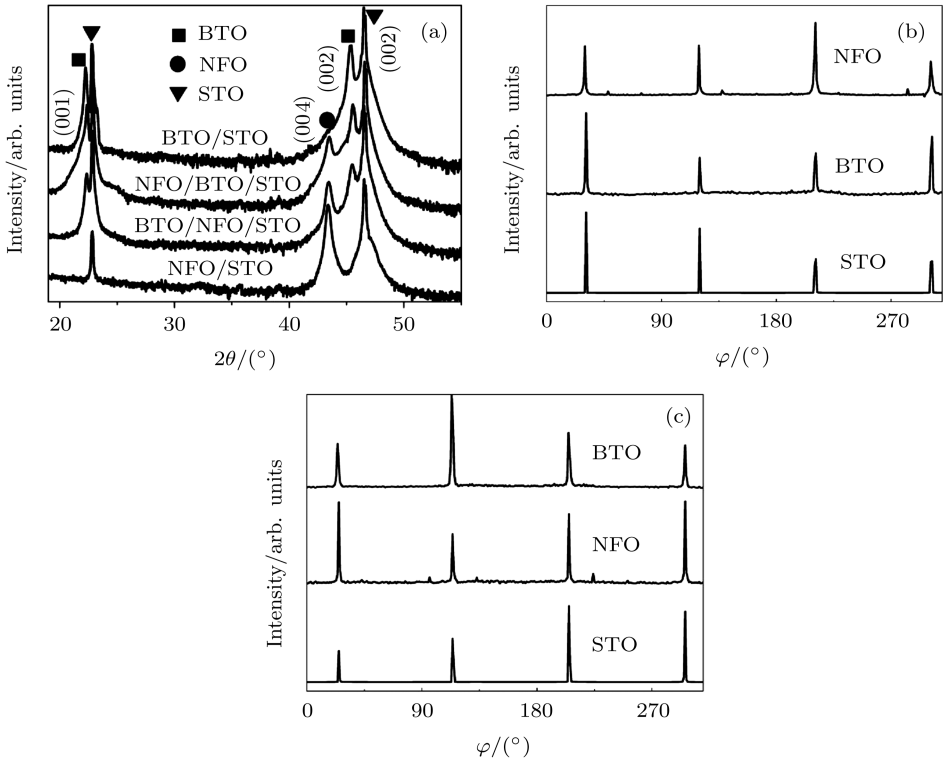


Fig.1. (a) X-ray diffraction patterns of the NFO-BTO composite thin films and single phase NFO and BTO films on the STO substrate, (b) intensity versus φ recorded on NFO (404), BTO (202), Nb:STO (202) reflections of NFO/BTO/STO heterostructure, and (c) intensity versus φ recorded on NFO (404), BTO (202), Nb:STO (202) reflections of BTO/NFO/STO heterostructure.

It is well known that there is an intrinsic similarity in crystal structure between perovskites and spinels, both of which have an octahedral oxygen coordination (see schematic illustration in Fig.2). This presents an opportunity to create a perovskite-spinel bilayer heterostructure. The lattice mismatch strain between NFO and STO in the BTO/NFO/STO heterostructure (see Fig.2(a)) is estimated to be $-6.3\%[=(2a_{\mathrm{STO}} - a_{\mathrm{NFO}})/a_{\mathrm{NFO}}]$ from the interface relationship discussed above, and this value is $-4.2\%[=(2a_{\mathrm{BTO}} - a_{\mathrm{NFO}})/a_{\mathrm{NFO}}]$ between NFO and BTO in the NFO/BTO/STO heterostructure (see Fig.2(b)). Thus, the NFO layers in both heterostructures would suffer compressive strains. These produce large strain energy stored at the interface, especially at the interface of NFO-STO. To reduce the total energy of the system, misfit edge dislocations would be generated at the interface (see Fig.3 below). By calculations from the XRD patterns (Fig.1), the average lattice parameters of the NFO layers are obtained to be 0.8331 and 0.8324 nm for the NFO/BTO/STO and the BTO/NFO/STO heterostructures, respectively, both of which are a bit smaller than that of bulk NFO (0.8337 nm from powder diffraction). Thus the average strains in the NFO layers are about –0.07% and –0.16% for the NFO/BTO/STO and BTO/NFO/STO heterostructures, respectively, indicating that the NFO layers are partly constrained by the substrate. Especially, the constraint strain in the NFO top layer is quite relaxed in the NFO/BTO/STO heterostructure.

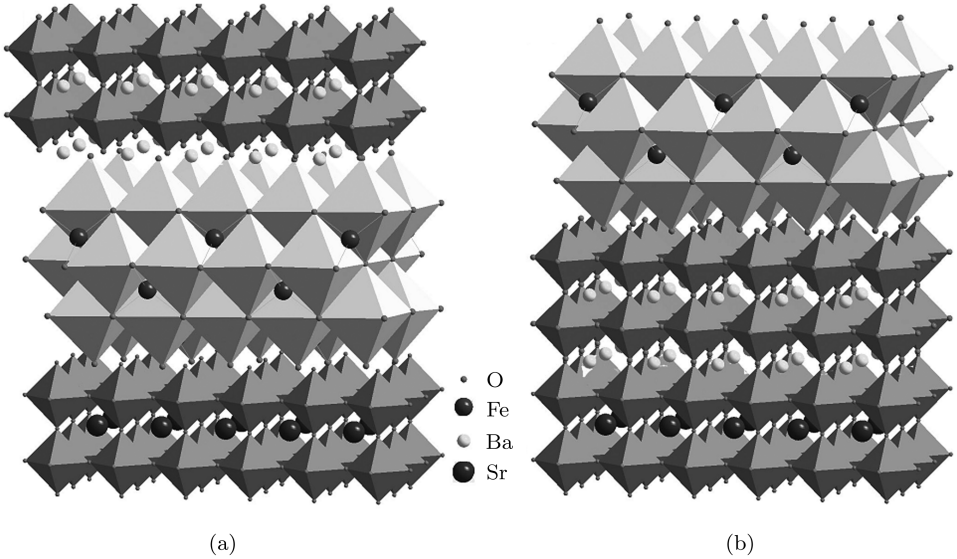


Fig.2. Schematic illustration of (a) heterostructure with a $BaTiO_3$ (top) and a $NiFe_2O_4$ (middle) on a $SrTiO_3$ substrate (bottom), and (b) heterostructure with a $NiFe_2O_4$ (top) and a $BaTiO_3$ (middle) on a $SrTiO_3$ substrate (bottom).

The epitaxially-grown heterostructures are also clearly evidenced further by HRTEM image (Fig.3). For example, Fig.3(a) shows a well-defined interface between the NFO and the BTO layers in the NFO/BTO/STO heterostructure. As seen from the corresponding selected-area electron diffraction (SAED) pattern in the inset of Fig.3(a), the sharp electron diffraction spots without any satellites or broadenings indicate that the films are of good single crystallinity. The interface relationship is [100]-NFO // [100]-BTO and (001)-NFO // (001)-BTO, which is consistent with the XRD results. This interface relationship suggests that the two layers have cube-on-cube epitaxy with respect to the substrate. Figure 3(b) shows the interface between the NFO layer and the STO substrate in the BTO/NFO/STO heterostructure. There are some edge dislocations forming over the entire interface, which are contributed to the release of strains as discussed above. The SAED pattern in the inset of Fig.3(b) also indicates the same interface relationship as that in the NFO/BTO/STO heterostructure, implying a cube-on-cube epitaxial growth. There is no evidence for any second phases or precipitates existing in the films or at the interface for both heterostructures.

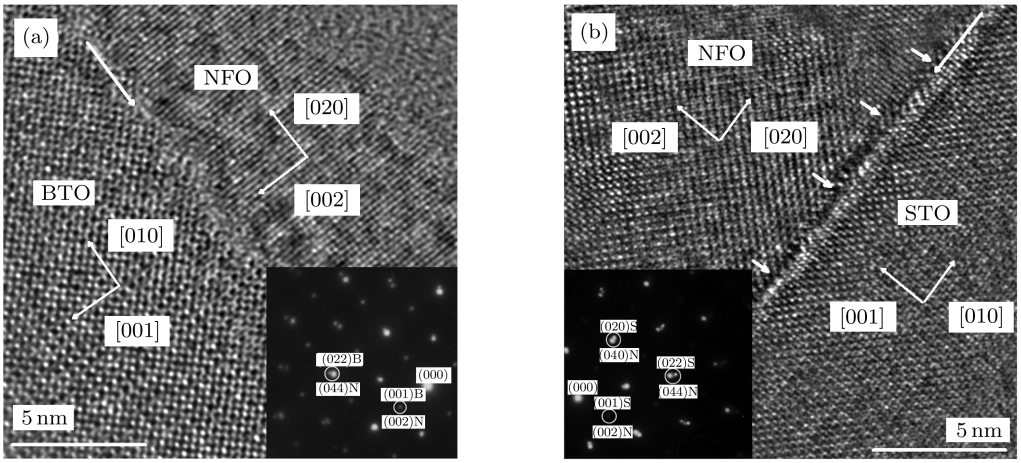


Fig.3. (a) HRTEM image for the NFO-BTO interface in the NFO/BTO/STO heterostructure, where the inset shows SAED from both NFO and BTO layers. (b) HRTEM image for the NFO-STO interface in the BTO/NFO/STO heterostructure, where the inset also shows SAED from both NFO and STO layers.

Both BTO/NFO/STO and NFO/BTO/STO heterostructures show an evident ferroelectric characteristic (Fig.4). The saturation polarization P_s and remnant polarization P_r are about 28 and 14 μC/cm^2 for the NFO/BTO/STO heterostructure, and about 33 and 19 μC/cm^2 for the BTO/NFO/STO heterostructure, respectively. These polarization values for the composite films are close to those for the pure BTO film (ca. 90 nm) deposited in the same way (see Fig.4), which are comparable to those for single crystal BTO.[18] It suggests that the heterostructured films have good ferroelectric properties. A slight imprint toward the negative electric field in these films is due to the inequivalence between the STO bottom electrode and the top Pt electrode. The coercive fields for the NFO/BTO/STO, BTO/NFO/STO, and pure BTO films are about 59, 46 and 64 MV/m, respectively, which are remarkably larger than that for single crystal BTO (ca. 0.1 MV/m). Generally, thin films have much higher coercive fields than anticipated values from the bulk data due to the constraint effect from substrate. In addition, the top and the bottom electrodes (i.e. Pt and STO) might be also attributed to the larger coercive fields.[19] It would bring a nearby-electrode injection that gives rise to an increase in coercive field for the Pt/Film/STO sandwiched structure. The large coercive fields further indicate that the rotation of the polarization is partly constrained by the stiff substrate. Due to the different constraint effects caused by the growth sequences of the BTO and the NFO layers, the coercive fields of these two heterostructures are different from each other. The larger coercive field of the NFO/BTO/STO heterostructure than that of the BTO/NFO/STO indicates that the BTO layer directly grown on the substrate in the NFO/BTO/STO heterostructure suffers more constraint strains than that deposited on NFO layer in the BTO/NFO/STO heterostructure.

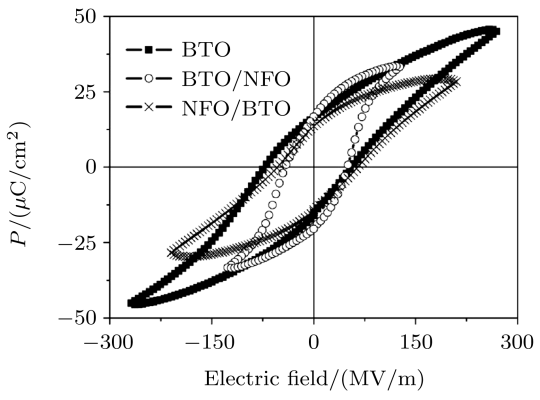


Fig.4. The ferroelectric hysteresis loops of the NFO-BTO composite film and the pure BTO film.

As shown in Fig.5, the values of saturation magnetization M_s are about 44 and 26 emu/cm^3 for the NFO/BTO/STO and BTO/NFO/STO heterostructured films, respectively. These magnetization values are close to that of the pure NFO film (i.e. 126 emu/cm^3) (1 emu = 10^{-3} A $\cdot$ m^2) if their saturation magnetization values are normalized only by the volume of the NFO layer rather than the whole volume of the composite films, indicating that the magnetization of the composite films is determined by the NFO layer and the NFO layer keeps its good magnetic quality in the heterostructured composite films. The values of coercive field H_c of the NFO/BTO/STO and BTO/NFO/STO heterostructures are about 230 and 600 Oe (1 Oe = 80 A/m), respectively, which are smaller than the value (i.e. about 820 Oe) for the pure NFO film deposited in the same way. The larger coercive field of the BTO/NFO/STO heterostructure than that of the NFO/BTO/STO heterostructure could be attributed to the larger constraint effect in the NFO bottom layer from the STO substrate as discussed above. Taking the BTO layer as the buffer layer, the constraint in NFO from the stiff substrate is evidently reduced in the NFO/BTO/STO heterostructure. The easier rotation of ferromagnetic domains in the NFO/BTO/STO than in the BTO/NFO/STO heterostructure would be advantageous for obtaining the visible ME effect.

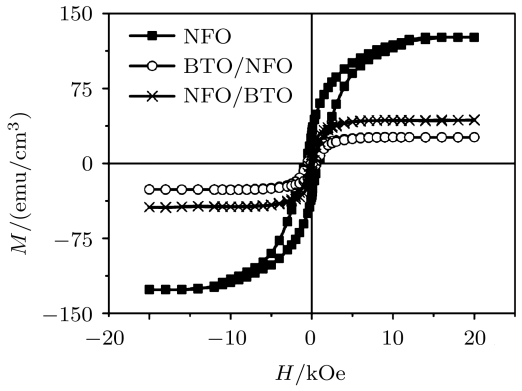


Fig.5. In-plane magnetic hysteresis loops of the NFO-BTO composite films and the pure NFO film (36 nm).

The good coexistence of ferroelectric and ferromagnetic behaviours as shown above offers a possibility to obtain an obvious ME effect. As shown in Fig.6, when an alternating magnetic field sig-

nal δH is applied, the single phase BTO and NFO films do not produce any values of ME output δV. In contrast, the heterostructured NFO/BTO/STO and BTO/NFO/STO films yield an obvious ME output following the magnetic excitation signal δH as shown in Fig.6(a). The ME output δV increases linearly with the ac magnetic field δH (Figs.6(b) and 6(c)), and the slopes give the ME voltage coefficients, $\alpha_{\mathrm{E}} = \delta V/(\delta H t)$ where t is the film thickness. Thus the out-of-plane and in-plane ME voltage coefficients for the NFO/BTO/STO heterostructure are respectively about 43.9 and 39.2 mV/cm Oe (1 Oe = 80 A/m) which are comparable with that for bulk composites.[20] The out-of-plane and the in-plane ME voltage coefficients for the BTO/NFO/STO heterostructure are about 5.3 and 4.9 mV/cm Oe, respectively. Larger ME voltage coefficients of the NFO/BTO/STO heterostructure than those of the BTO/NFO/STO heterostructure are due to smaller constraint in the NFO layer of the former than the latter heterostructure as discussed above, i.e. the better released NFO top layer in the NFO/BTO/STO heterostructure is responsible for its larger ME voltage coefficient.

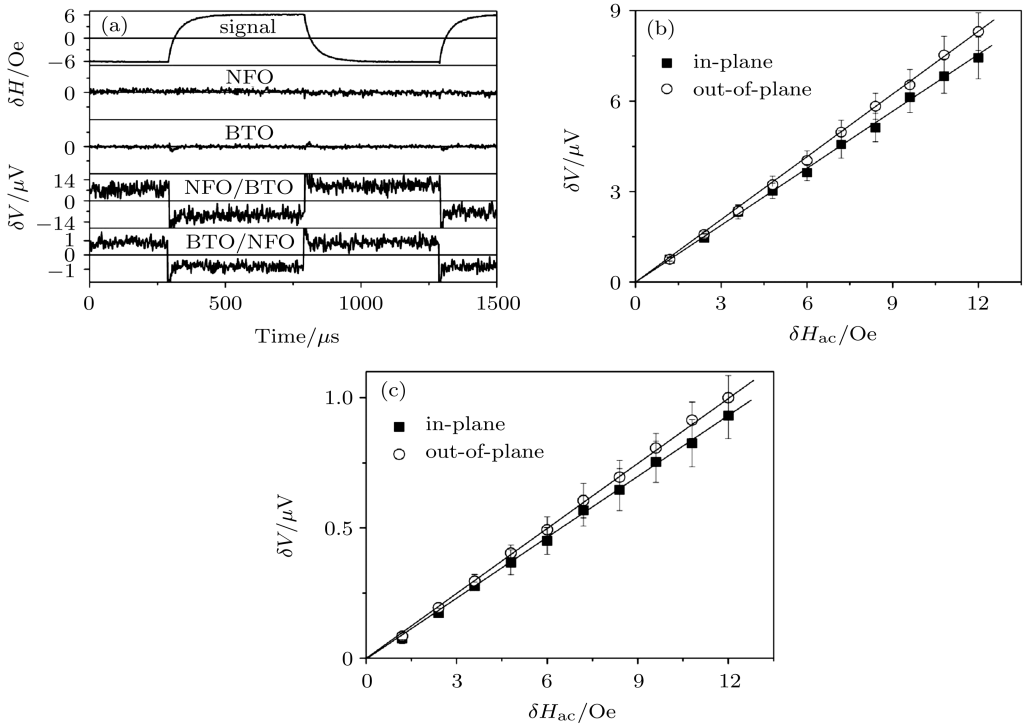


Fig.6. The ME response of the films with the in-plane magnetic field applied and the input signal δH being a 1 kHz square wave (a) and the induced ME signal δV as a function of ac magnetic field δH at 1 kHz with a bias magnetic field 100 Oe for the NFO/BTO/STO heterostructure (b) and the BTO/NFO/STO heterostructure (c).

By comparison with the vertical heterostructures, such horizontal heterostructures suffer large in-plane constraint from rigid substrates. The in-plane constraint in the NFO layer would affect the ME output in the horizontal heterostructures. The induced voltage changes [i.e. $\Delta V = V(H_{\mathrm{dc}}) - V(H_{\mathrm{dc}} = 0)$] by the applied magnetic bias H_{dc} in these two BTO-NFO heteroepitaxies are small, i.e. about 120 nV and 80 nV for the heterostructured NFO/BTO/STO and BTO/NFO/STO films respectively, when $H_{\mathrm{dc}} =$ 5.5 kOe. The changes of small bias-induced voltage in these two heterostructures are attributed to the clamping effect inherent in the heteroepitaxy, where the in-plane constraint effect inhibits the magnetostriction of NFO. On the other hand, the saturation magnetostriction of NFO itself is about –10 ppm (0.001%) which is much smaller than the residual strains (i.e. ca 0.1%) in the NFO layers of both heterostructures.

4. Conclusions

Two heterostructured NFO-BTO multiferroic composite films with different growth sequences, i.e. NFO/BTO/STO and BTO/NFO/STO, have

been grown. The different growth modes of BTO and NFO on different bottom layers/substrate lead to different morphologies of these two heterostructures, and thus their different multiferroic behaviours. Both heterostructures indicate the good coexistence of ferroelectric and ferromagnetic behaviours, and the obvious direct ME effect has been observed in both heterostructures. By releasing more constraints in the magnetic layer from the substrate, the NFO/BTO/STO heterostructure demonstrates better ME response.

References

[1] Eerenstein W, Mathur N D and Scott J F 2006 *Nature* **442** 759

[2] Fiebig M 2005 *J. Phys.* D: *Appl. Phys.* **38** R123

[3] Nan C W 1994 *Phys. Rev.* B **50** 6082

[4] Nan C W, Liu L, Cai N, Zhai J, Ye Y, Lin Y H, Dong L J and Xiong C X 2002 *Appl. Phys. Lett.* **81** 3831

[5] Dong S X, Cheng J R, Li J F and Viehland D 2003 *Appl. Phys. Lett.* **83** 4812

[6] Cai N, Zhai J Y, Shi Z, Lin Y H and Nan C W 2004 *Chin. Phys.* **13** 1348

[7] Zhang R, Wang M, Zhang N and Srinivasan G 2006 *Acta Phys. Sin.* **55** 2548

[8] Zheng H, Wang J, Lofland S E, Ma Z, Mohaddes-Ardabili L, Zhao T, Salamanca-Riba L, Shinde S R, Ogale S B, Bai F, Viehland D, Jia Y, Schlom D G, Wuttig M, Roytburd A and Ramesh R 2004 *Science* **303** 661

[9] Zavaliche F, Zheng H, Mohaddes-Ardabili L, Yang S Y, Zhan Q, Shafer P, Reilly E, Chopdekar R, Jia Y, Wright P, Schlom D G, Suzuki Y and Ramesh R 2005 *Nano Lett.* **5** 1793

[10] Nan C W, Liu G, Lin Y H and Chen H D 2005 *Phys. Rev. Lett.* **94** 197203

[11] Zhang J X, Li Y L, Schlom D G, Chen L Q, Zavaliche F, Ramesh R and Jia Q X 2007 *Appl. Phys. Lett.* **90** 052909

[12] Zhou J P, Shi Z, Liu G, He H C and Nan C W 2006 *Acta Phys. Sin.* **55** 3766

[13] Deng C Y, Zhang Yi, Ma Jing, Lin Y H and Nan C W 2007 *J. Appl. Phys.* **102** 074114

[14] Eerenstein W, Wiora M, Prieto J L, Scott J F and Mathur N D 2007 *Nat. Mater.* **6** 348

[15] He H C, Wang J, Zhou B P and Nan C W 2007 *Adv. Funct. Mater.* **17** 1333

[16] Ma Y G, Cheng W N, Ning M and Ong C K 2007 *Appl. Phys. Lett.* **90** 152911

[17] Levin I, Li J H, Slutsker J and Roytburd A L 2006 *Adv. Mater.* **18** 2044

[18] Sharma H B, Sarma H N K and Mansingh A 1999 *J. Mater. Sci.* **34** 1385

[19] Tagantsev A K and Stolichnov I A 1999 *Appl. Phys. Lett.***74** 1326

[20] Zhai J Y, Cai N, Shi Z, Lin Y H and Nan C W 2004 *J. Appl. Phys.* **95** 5685